

# Gold Nanoparticle Films As Sensitive and Reusable Elemental Mercury Sensors

Jay Z. James,<sup>†</sup> Donald Lucas,<sup>‡,\*</sup> and Catherine P. Koshland<sup>§</sup>

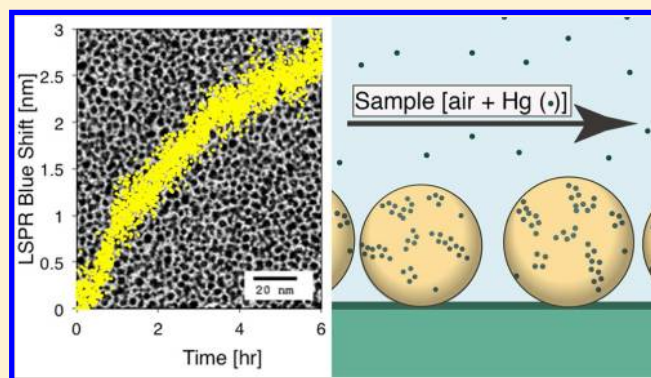
<sup>†</sup>Department of Mechanical Engineering, University of California at Berkeley,

<sup>‡</sup>Environmental Energy Technologies Division, Lawrence Berkeley National Laboratory,

<sup>§</sup>School of Public Health, University of California at Berkeley, Berkeley, California 94720, United States

## Supporting Information

**ABSTRACT:** We demonstrate the utility of gold nanoparticles (AuNPs) as the basis of a stand-alone, inexpensive, and sensitive mercury monitor. Gold nanoparticles absorb visible light due to localized surface plasmon resonance (LSPR), and the absorbance changes when mercury combines with the gold nanoparticles. The sensitivity of the peak absorbance is proportional to the surface-area-to-volume ratio. We chose 5 nm spheres because they have the largest surface-area-to-volume ratio while still having a peak absorption in the visible range. The adsorption of 15 atoms of Hg causes a 1 nm shift in the LSPR wavelength of these particles. Assembled into a film using the Langmuir–Blodgett method, the AuNP LSPR can be tracked with a simple UV–vis spectrometer. The rate of shift in the peak absorbance is linear with mercury concentrations from 1 to 825  $\mu\text{g}_{\text{Hg}}/\text{m}_{\text{air}}^3$ . Increasing the flow velocity (and mass transfer rate) increases the peak shift rate making this system a viable method for direct ambient mercury vapor measurements. Regeneration of the sensing films, done by heating to 160 °C, allows for repeatable measurements on the same film.



## INTRODUCTION

Mercury, a neurotoxic global pollutant, demands global regulation. The long lifetime of mercury in the atmosphere (>1 year) allows long-range transport limiting local emission controls from protecting all environments. Policy makers are working toward a worldwide effort similar to the sulfur dioxide or CFC regulations of the 20th century. Anticipating a global policy, the European Commission began a five-year project in 2010 called the Global Mercury Observation System (GMOS, [www.gmos.eu](http://www.gmos.eu)) to create a coordinated global network adequate for improving models and making policy recommendations. The new system expands on the regional efforts made in North America (i.e., the Mercury Deposit Network and North American Airborne Mercury Experiment) and the independent observations made around the world. A preliminary assessment by GMOS points to gaps in emissions monitoring and in the spatial coverage of environmental observations, mostly in the southern hemisphere. Lack of an inexpensive, stand-alone, low-power, low-maintenance sensor is a primary technical issue confronting the GMOS.

Current air monitors are amply sensitive to detect the global background (1.2  $\text{ng}/\text{m}^3$ ) but are costly and high maintenance.<sup>1</sup> Preconcentration of trace mercury vapor samples is required for ambient measurements and depends on gold surfaces to effectively trap and quickly release mercury in detectable amounts. Concentrations as low as 0.1  $\text{ng}/\text{m}^3$  can be analyzed

using a trap made of gold-coated sand that feeds a cold vapor atomic fluorescence or absorption spectroscopy.<sup>2,3</sup>

Beyond providing selective adsorption for sample collection, gold performs as a transducer for mercury in various measurement techniques. Thundat et al. (1995) demonstrated the quantitative detection of adsorbed mercury with gold-coated microcantilevers.<sup>4</sup> Picogram resolution was obtained by monitoring changes in the resonant frequency of the cantilever bending. Resistivity changes in gold films are proportional to the adsorbed mercury mass,<sup>5</sup> an effect utilized by commercially available mercury vapor analyzers with  $\sim\mu\text{g}_{\text{Hg}}/\text{m}_{\text{air}}^3$  resolution. Adsorbed mercury also induces changes in the optical properties of gold films, measurable with surface plasmon resonance spectroscopy.<sup>6</sup> In nanoparticle form, the optical property changes can be followed with simple and inexpensive visible light absorbance spectroscopy. Metal nanoparticles exhibit peaks in absorbance due to localized surface plasmon resonance (LSPR). The location of the peak depends on shape, size, composition, and local environment. Adsorption of mercury alters a gold nanoparticle's complex dielectric function and causes a blue shift in the LSPR wavelength, seen in both

Received: February 9, 2012

Revised: June 18, 2012

Accepted: August 7, 2012

Published: August 7, 2012

colloidal solutions<sup>7–10</sup> and films.<sup>11,12</sup> Our recent work studying the LSPR response of individual gold nanorods achieved attogram ( $10^{-15}$  g) resolution and found the sensitivity to be proportional to the nanoparticle's surface-area-to-volume ratio.<sup>13</sup> Responding to the technical needs of an expanding mercury observation network, we are developing a reliable, sensitive, and inexpensive method for LSPR-based mercury detection.

## ■ EXPERIMENTAL SECTION

**Nanoparticle Film Preparation.** Quartz, diced in 9 mm squares, acts as the transparent substrate for the nanoparticle film. Before use, the quartz surfaces were cleaned in piranha solution for 15 min, (**Caution!** Piranha is a strong oxidizer and should not be stored in closed containers) rinsed in water (18.2 M $\Omega$ , Millipore) and ethanol, and dried in nitrogen. We used commercially available 4-*tert*-butylthiophenol functionalized 2–5 nm gold nanoparticles (Alfa Aesar). Particle measurements (ImageJ) from the TEM images reveal the particles to have an average diameter of 4.3 nm with a standard deviation of 2.5 nm. A histogram of the nanoparticle size distribution is available in the Supporting Information. The nanoparticles were suspended in chloroform and deposited, dropwise, onto the water surface held by a Teflon Langmuir–Blodgett trough (Nima). After 30 min, the film was compressed, using the motorized Teflon barrier, to 15 mN/m surface pressure. The particle monolayer forms while floating on the aqueous subphase, controlled by the uniaxial compression of the trough surface area. The substrate dipper then drew the submerged quartz chips and TEM grids (silicon nitride, Ted Pella) through the floating nanoparticle layer fixing the particles to the substrate surfaces while the barrier holds the film at a uniform compression.

**Film Characterization.** TEM imaging (H-7650, Hitachi) and UV–vis absorption spectroscopy (HR4000, Ocean Optics) provided characterization of the particle films. A Lorentzian curve, fitted to the recorded spectra using Matlab, located the peak wavelength of the LSPR with a resolution of 0.5 nm.

**Sample Bag Method.** Initial exposures to mercury vapor employed a Teflon sample bag (SKC) with a controlled dilution of saturated mercury vapor in clean air (Zero Air, AirGas). A peristaltic pump drew the sample from the bag over the sensor chip at a constant flow of 15 cc/min. A quartz flow cell (Starna Cells) held the sensor chip for in situ recording of the absorbance spectra. Each spectrum saved is the average of 100 spectra with integration times of 80 ms. This technique was used for samples ranging from 25 to 825  $\mu\text{g}_{\text{Hg}}/\text{m}_{\text{air}}^3$ . The concentration of each dilution was measured using a conductometric mercury analyzer with an accuracy of  $\pm 5\%$  (Jerome J405).

**Permeation Tube Method.** For higher flow rates and lower concentrations a chip was affixed with a silicone adhesive to a 1.25 cm inner-diameter Pyrex tube such that the film faced normal to the axis of the tube. The collimating lenses and tube were held in a fixed position with the beam perpendicular to the sensor chip, ensuring observation of a consistent area of the chip during the absorbance measurements.

A permeation tube (VICI Metronics) in a steady flow of air supplied a constant mercury concentration for the higher flow rates. The emission of Hg from the permeation tube is constant for a given temperature with 60 ng/s emitted at room temperature (295 K). In a stream of 57 L per minute (LPM) of air, the permeation tube system provides  $1.05 \mu\text{g}_{\text{Hg}}/\text{m}_{\text{air}}^3$ .

**Regeneration.** Heating tape, wrapped about the tube and connected to an autotransformer, was used to regenerate the sensor. A low flow of mercury free air (6 LPM) during heating purged the system. A low temperature (433 K) for regeneration kept the nanoparticles from coalescing allowing reuse of the film for further measurements.

## ■ RESULTS AND DISCUSSION

Optimizing LSPR-based mercury sensing requires choosing the best material for selective adsorption and sensitive response. We used gold because it is a selective and stable mercury adsorbing material<sup>14,15</sup> and can be grown in a variety of shapes and sizes of nanoparticles.<sup>16</sup> We then determined the most sensitive and stable gold nanoparticle from available shapes and sizes. Morris et al. exposed films of gold nanospheres of varying size to saturated mercury vapor in room temperature air.<sup>12</sup> They found that the shifts in LSPR at saturation were greater for smaller particles. Our previous work observing individual gold nanorods' spectral response to  $\mu\text{g}/\text{m}^3$  concentrations of mercury in air found that the sensitivity was not dependent on size directly, but proportional to surface-area-to-volume ratio.<sup>13</sup> We selected  $\sim 5$  nm spheres because they have the largest surface-area-to-volume ratio while still having an observable peak in absorbance for an assembled film.<sup>12</sup> A schematic of the sensor is shown in Figure 1. Spheres are the minimum surface-

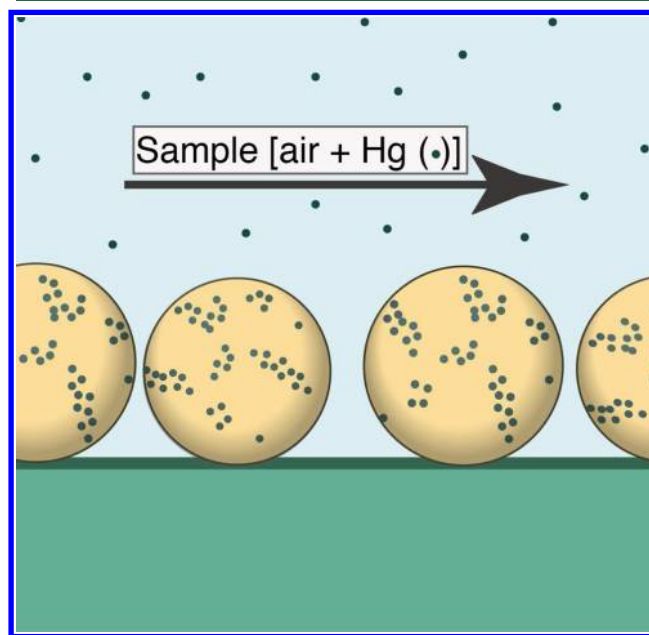


**Figure 1.** Schematic of gold nanoparticle film during exposure to mercury vapor.

area-to-volume ratio shape but they can be synthesized in much smaller sizes than the more complicated geometries. Being the minimum surface-area-to-volume geometry also serves as an advantage for the shape stability of spheroid particles.

The response of a 5 nm AuNP's LSPR to amalgamation can be predicted with the use of existing models and previous experiments. The LSPR wavelength of bimetallic nanoparticles shifts proportionally to alloying mass fraction.<sup>17</sup> Because of differences in the complex dielectric, a 5 nm Hg particle LSPR wavelength would be 273 nm, 240 nm shorter than a AuNP of the same size. The Link et al. model predicts a shift of 2.4 nm for each percentage increase in the Hg mass fraction, which in

the case of the 5 nm sphere is equivalent to 38 atoms of Hg. The model agrees with experimental observations comparing UV–vis spectra with the measured mass fraction.<sup>7,10,13</sup>

Whereas we have observed the spectra of individual nanoparticles, both AuNP and amalgam particles, with dark field spectroscopy, for a practical sensor we measure the spectral response of an array of particles using UV–vis absorbance spectroscopy. Assembly of such a particle film can be done in a variety of ways. We decided to use the Langmuir–Blodgett method because we can manufacture nanoparticle films in a controlled, parallel, inexpensive fashion.<sup>18</sup> TEM images show the AuNP-film to be near close-packed with particles having an average diameter of 4.3 nm. A typical TEM image is shown in part a of Figure 2. An average density of particles found in the TEM images from different locations on the grid (using ImageJ's particle counting routine) was used to approximate the total number of particle on the sensor chip. The result suggests that there are about  $2 \times 10^{12}$  particles (18  $\mu\text{g}$ ) on each  $1 \text{ cm}^2$  chip. The close proximity of the particles allows coupling between neighboring plasmons driving the resonance to longer wavelengths (isolated particles have an LSPR wavelength of  $\sim 520 \text{ nm}$ ).<sup>19,20</sup> The red shift in the LSPR is accompanied by a peak broadening shown in part b of Figure 2. All films tested originate from the same Langmuir–Blodgett batch and have an average LSPR wavelength of 547.5 nm. Films exposed to mercury vapor exhibit a blue shift in their LSPR wavelength that slows as the chip saturates as in Figure 3.

The LSPR shift as a function of time (Figure 3) represents an integral of mercury concentration. Thus, a time derivative of the LSPR shift corresponds to a continuous measurement of concentration. Exposed to varying concentrations of Hg in air, the films generated using the Langmuir–Blodgett technique blue shift faster for higher concentrations. Using a flow rate of 15 cc/min and mercury concentrations ranging from 25 to 825  $\mu\text{g}_{\text{Hg}}/\text{m}_{\text{air}}^3$  the initial LSPR shift rates ( $\nu_{\text{LSPR}}$ ) are proportional to the sample concentrations. We used a linear fit of the first 2 nm of the peak's blue shift to determine the initial  $\nu_{\text{LSPR}}$ . The shift rates for 5 films exposed to a range of concentrations show a correlation in part a of Figure 4. A linear regression of the mercury concentration dependence of  $\nu_{\text{LSPR}}$ , fixed at the origin, predicts each  $\mu\text{g}_{\text{Hg}}/\text{m}_{\text{air}}^3$  increase in sample concentration will result in a 0.023 nm/h increase in  $\nu_{\text{LSPR}}$ .

The sensitivity of the sensor depends on the interparticle distance within the film. Despite controlling for a constant surface pressure during the deposition (15 mN/m), the prepared films have varying initial LSPR wavelengths (541.5–550 nm). The longer LSPR wavelengths correspond to greater coupling between the nanoparticles in the film caused by smaller interparticle spacing.<sup>20</sup> Because the films were exposed to different mercury concentrations, we use a normalized  $\nu_{\text{LSPR}}$  as a proxy for the sensitivity. The normalized  $\nu_{\text{LSPR}}$  is the ratio of the  $\nu_{\text{LSPR}}$  and the mercury concentration, and has units of nm/h/ $(\mu\text{g}/\text{m}^3)$ . Plotted in part b of Figure 4, the shorter initial LSPR wavelengths show greater sensitivity with the normalized  $\nu_{\text{LSPR}}$  decreasing 67% in the range of initial LSPR tested. The decrease in sensitivity can be attributed to a combination of mass transfer and optical effects. In terms of the latter, the data suggest that plasmon coupling arising from closely spaced nanoparticles reduces the sensitivity of the film LSPR to adsorbed mercury mass. Given a probed area of fixed dimensions, the number of particles decreases with increasing interparticle spacing. Probing fewer particles reduces the mass sensitivity of the sensor. Increased interparticle spacing within

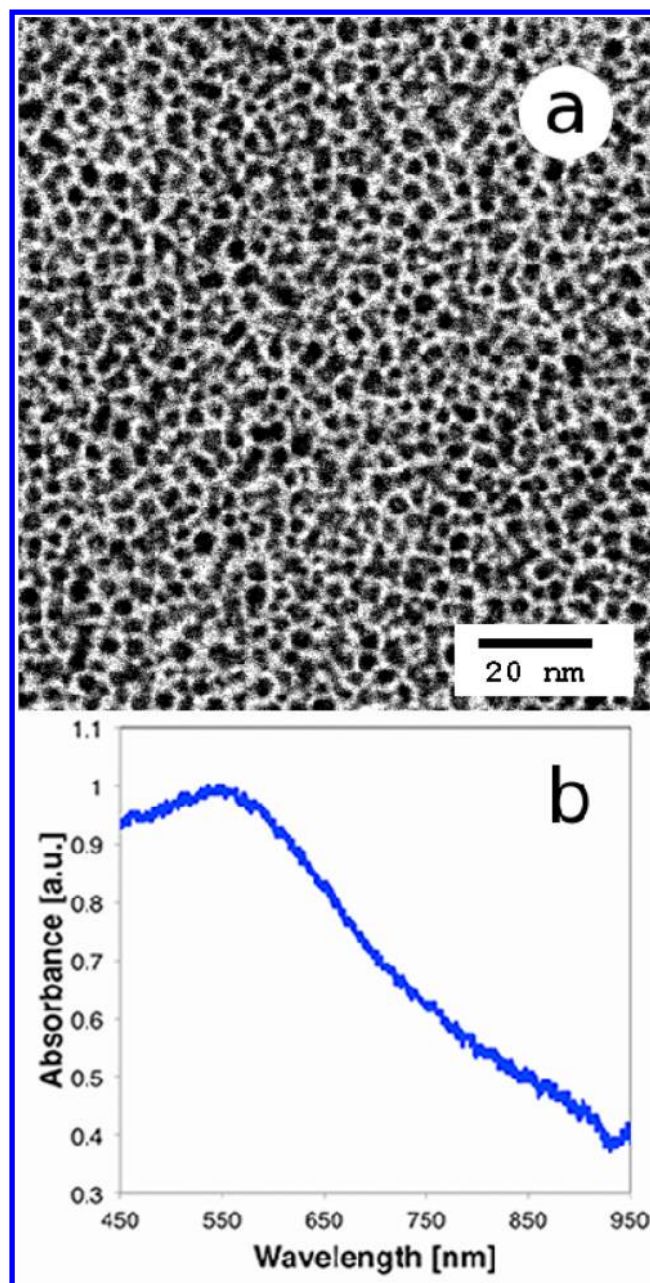


**Figure 2.** (a) TEM image of the Langmuir–Blodgett generated film showing the particle sizes and distribution in film. (b) A typical UV–vis absorption of the nanoparticle film on quartz. The film's LSPR wavelength is 550 nm.

the range tested here should increase the mass flux of mercury per particle. Adsorption at neighboring particles depletes the local concentration retarding adsorptive flux per particle. The results support using a lower surface pressure during deposition to generate more disperse films. Tao et al. (2007) previously demonstrated the role of surface pressure during the Langmuir–Blodgett deposition in determining the packing density of silver nanoparticles.<sup>21</sup> By reducing the surface pressure to 8 mN/m, we were able to reduce the packing density and create films with resonant absorbance at  $\sim 520 \text{ nm}$ . A representative absorbance spectrum and TEM image of these less-dense films are available in the Supporting Information.

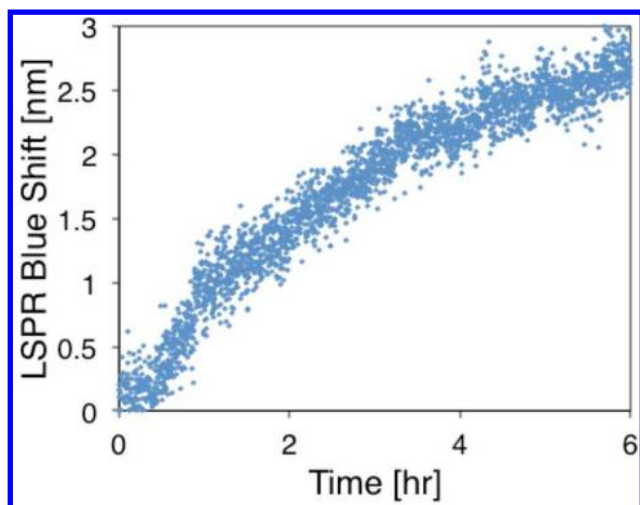


**Figure 3.** Time trace of relative LSPR peak position during exposure to mercury vapor ( $3 \mu\text{g}/\text{m}^3$  @ 20 LPM). A linear fit to the first nanometer of shift is used to determine  $v_{\text{LSPR}}$  for the run.

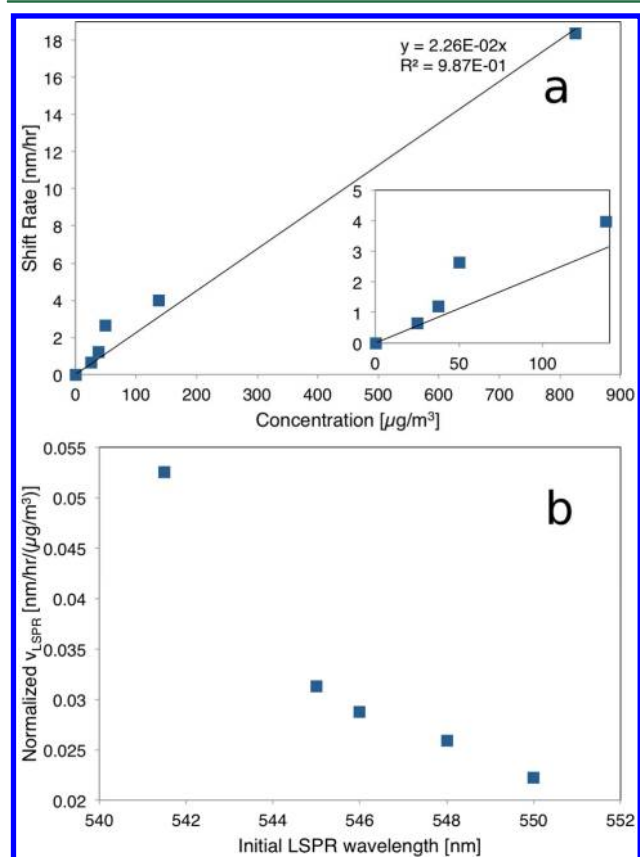


**Figure 4.** (a) Calibration curve generated using nanoparticle films exposed to a constant stream of 15 cc/min mercury vapor (20–825  $\mu\text{g}/\text{m}^3$ ) with an insert magnifying the results from lower concentration exposures. (b) The same experimental results as (a) but plotted to show the dependence of the  $v_{\text{LSPR}}$  on the initial LSPR wavelength. Normalized  $v_{\text{LSPR}}$  is ratio of the measured  $v_{\text{LSPR}}$  to the mercury vapor concentration.

The  $v_{\text{LSPR}}$  is also proportional to the rate of mercury adsorption, which is controlled by the diffusive mass transfer of the trace mercury vapor. The mass transfer rate determines the time resolution of the sensor and can be controlled through engineering the exposure conditions. Increasing the sample

flow rate reduces the collection times for low concentration measurements. For a flat surface introduced into a uniform flow field, flowing parallel to the surface, the mass transfer at the surface for a single dissolved species can be solved analytically if the surface concentration is known and the flow remains laminar. Elemental mercury vapor has a high affinity for gold, with an observed sticking coefficient of approximately one. This allows the assumption that the mercury vapor concentration at the gold boundary is zero. The solution predicts a mass transfer rate proportional to the square root of the bulk velocity, and linear with the mercury concentration. However, the square root dependence does not hold for turbulent flows. Experiments using the same geometry with turbulent flows show that the mass transfer rate remains directly proportional to concentration and proportional to the fluid's Reynolds number to a power ranging between 0.8 and 1.

The need for continuous measurements and remote operation make a single-use sensor chip limited in appeal. It is well-known that bulk gold releases mercury when heated to above 373 K, and the surface can be regenerated to collect gold in a repeatable fashion. It is not clear that gold nanoparticles have the same property, especially for nonspherical shapes. We found that gentle heating of the amalgam nanoparticle film evolves mercury as a vapor. The sensor response to mercury exposure following an hour at 433 K was consistent, with no degradation observed for more than 30 regenerations. This process is similar to the preconcentration of mercury samples using a gold trap, but at a lower temperature. The bulk gold films used in the traps are more structurally stable and can survive the 1173 K temperatures they are commonly heated to during the evolution step. Preservation of the nanoparticle film morphology is key to a reproducible LSPR response; the melting point is size dependent and melting point depression in nanoparticles makes the nanoparticle film vulnerable to lower temperatures than bulk gold. The depression is nonlinear with particle dimension, greatly impacting the melting temperature of our 4.3 nm particles.<sup>22</sup> Heating to 513 K for one hour causes irreversible changes to the film wherein the particles coalesce forming larger particles ( $d = 8 \text{ nm}$ ). A TEM image of one such film is shown in Figure 5. The larger diameter particles show a 50% reduction in sensitivity to mercury vapor, due in part to a reduction of the surface-area-to-volume ratio.

A single sensor chip was used in a series of exposures and regenerations to test the precision of the method and its agreement with flow rate trends of the mass transfer model. For six runs done with a flow rate and concentration of 20 LPM and  $3 \mu\text{g}/\text{m}^3$ , the  $v_{\text{LSPR}}$  was 1.1 nm/hour on average with a standard deviation of 7%. Increasing the flow rate to 57 LPM with a sample of  $1 \mu\text{g}_{\text{Hg}}/\text{m}_{\text{air}}^3$  the  $v_{\text{LSPR}}$  was 0.42 nm/hour. For flow rates below 40 LPM, the flow in the Pyrex tube is laminar. Figure 6 demonstrates good agreement between the mass transfer model and the experimental data by normalizing  $v_{\text{LSPR}}$  to a single concentration ( $1 \text{ ng}_{\text{Hg}}/\text{m}_{\text{air}}^3$ , a typical ambient concentration<sup>23</sup>). The experimental results follow a square root dependence on flow rate for flows up to 40 LPM, but for 57 LPM flow (which is expected to be turbulent ( $\text{Re} = 3584$ )) the  $v_{\text{LSPR}}$  is three times faster than the laminar trend predicts. The time resolution of LSPR sensing of ambient mercury needs to be competitive with the existing methods, some of which take 24 h of collection. The time resolution is limited by the rate of adsorption, which increases with Reynolds number. At the greatest flow rate tested, 57 LPM, an ambient mercury measurement ( $1 \text{ ng}_{\text{Hg}}/\text{m}_{\text{air}}^3$ ) would take 410 h to shift 1 nm.

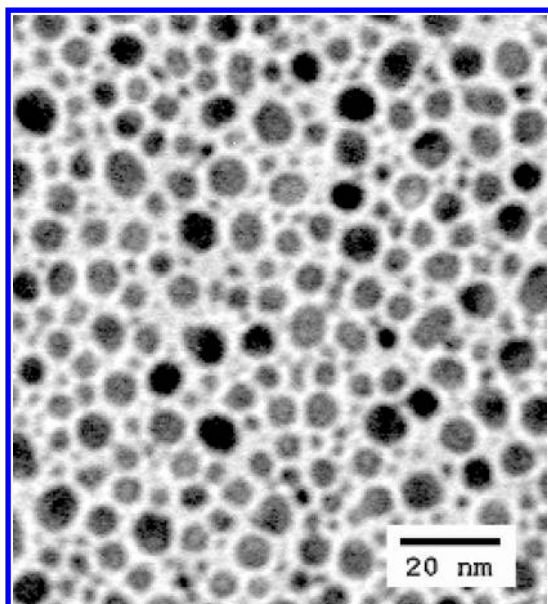


**Figure 5.** TEM image of nanoparticle film showing irreversible changes following heating to 513 K for 1 h.

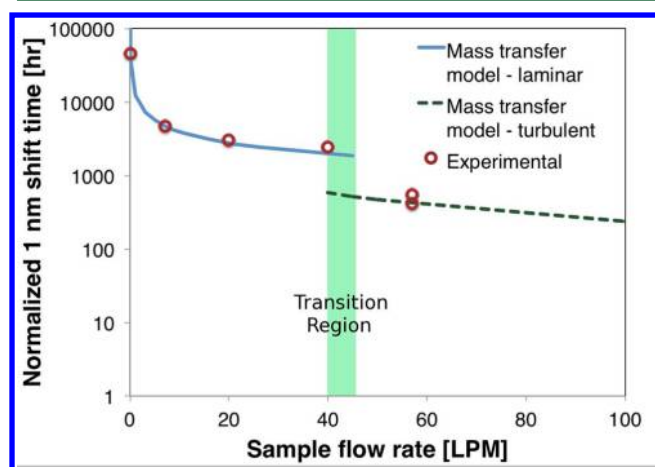


**Figure 6.** Normalization of all tests to a single concentration ( $1 \text{ ng}/\text{m}^3$ ) to demonstrate the effect of the sample flow rate. The experimental data (open circles) overlaid on the mass transfer models, laminar (solid line), and turbulent (dashed line).

By accelerating the flow rate or implementing an impinging flow, the time resolution can be reduced dramatically.

Accuracy of the sensor can be improved by controlling for the confounding factors. Observation of LSPR temperature dependence during the heating and cooling steps of regeneration prompted the use of a thermocouple to monitor the sensor temperature. A linear regression of the LSPR versus temperature data from the hour before exposure allows normalization of the peak position; the LSPR peak temperature dependence was  $1.7 \text{ nm}/\text{K}$ . Additional confounding effects appear as a gradual red shifting ( $0.02 \text{ nm}/\text{h}$ ) of the LSPR for mercury free sample air. This is likely due to other adsorbates that increase the index of refraction surrounding the AuNPs causing the shift of the resonance to longer wavelengths. No efforts were made to correct for the red shifts, as they are slower than the standard deviation of the sensor response to the tested mercury concentrations (7%). Confounding effects will increase with respect to the mercury signal at lower

concentrations but have been mitigated through the use of protective monolayer films on similar gold film based sensors.<sup>24</sup>

With the aim of developing a highly sensitive and inexpensive mercury vapor sensor we employed a film of  $\sim 5 \text{ nm}$  AuNPs in an LSPR-based chemical sensor. AuNP films act as both receptors and transducers by selectively adsorbing mercury vapor and changing their visible absorption spectra. Response to concentrations between  $1$  to  $825 \mu\text{g}_{\text{Hg}}/\text{m}_{\text{air}}^3$  confirms that the LSPR method is equivalently sensitive to current commercial methods. Adsorption of  $15 \text{ Hg}$  atoms per nanoparticle causes a  $1 \text{ nm}$  shift in LSPR wavelength, twice the error of our Lorentzian peak measurement ( $0.5 \text{ nm}$ ). Multiplying the number of Hg atoms per particle by the number of particles in the optical path ( $2 \times 10^{12} \text{ particles}/\text{cm}^2$  in an area of  $\sim 1 \text{ mm}^2$ ) yields  $100 \text{ picograms}$  of mercury causing the observed changes. Simple heating of the film causes a reversible desorption of mercury. The cost of such a monitor comprised of a AuNP film, heater, pump, lamp, and appropriate spectrometer is considerably less than the methods used now.

## ■ ASSOCIATED CONTENT

### 📄 Supporting Information

TEM images, and UV–vis absorbance data. This material is available free of charge via the Internet at <http://pubs.acs.org>.

## ■ AUTHOR INFORMATION

### Corresponding Author

\*E-mail: [d\\_lucas@lbl.gov](mailto:d_lucas@lbl.gov).

### Notes

The authors declare no competing financial interest.

## ■ ACKNOWLEDGMENTS

This project was supported by Award Number P42ES004705 from NIEHS and the Wood-Calvert Chair. The content is solely the responsibility of the authors and does not necessarily represent the official views of NIEHS or NIH.

## ■ REFERENCES

- (1) French, N. B.; Priebe, S. J.; Haas, W. J., Jr. Product reviews: State-of-the-art mercury CEMs. *Anal. Chem.* **1999**, *71*, 470A–475A.
- (2) Hatch, W. R.; Ott, W. L. Determination of submicrogram quantities of mercury by atomic absorption spectrophotometry. *Anal. Chem.* **1968**, *40*, 2085–2087.
- (3) Muscat, V. I.; Vickers, T. J.; Andren, A. Simple and versatile atomic fluorescence system for determination of nanogram quantities of mercury. *Anal. Chem.* **1972**, *44*, 218–221.
- (4) Thundat, T.; Wachter, E.; Sharp, S.; Warmack, R. Detection of mercury-vapor using resonating microcantilevers. *Appl. Phys. Lett.* **1995**, *66*, 1695–1697.
- (5) McNerney, J. J.; Buseck, P. R.; Hanson, R. C. Mercury detection by means of thin gold films. *Science* **1972**, *178*, 611–612.
- (6) Morris, T.; Szulczewski, G. Evaluating the role of coinage metal films in the detection of mercury vapor by surface plasmon resonance spectroscopy. *Langmuir* **2002**, *18*, 5823–5829.
- (7) Morris, T.; Copeland, H.; McLinden, E.; Wilson, S.; Szulczewski, G. The effects of mercury adsorption on the optical response of size-selected gold and silver nanoparticles. *Langmuir* **2002**, *18*, 7261–7264.
- (8) Scallan, K.; Lucas, D.; Koshland, C. A novel UV-vis spectroscopic method to detect elemental mercury using gold nanoparticles. *Epidemiology* **2006**, *17*.
- (9) Rex, M.; Hernandez, F. E.; Campiglia, A. D. Pushing the limits of mercury sensors with gold nanorods. *Anal. Chem.* **2006**, *78*, 445–451.
- (10) Mertens, S. F. L.; Gara, M.; Sologubenko, A. S.; Mayer, J.; Szidat, S.; Krämer, K. W.; Jacob, T.; Schiffrin, D. J.; Wandlowski, T. Gold–mercury nanoalloys: Au@Hg nanoalloy formation through

direct amalgamation: Structural, spectroscopic, and computational evidence for slow nanoscale diffusion (*Adv. Funct. Mater.* 17/2011). *Adv. Funct. Mater.* **2011**, *21*, 3202.

(11) Wang, C.; Ma, L.; Hossain, M.; Wang, H.; Zou, S.; Hickman, J. J.; Su, M. Direct visualization of molecular scale chemical adsorptions on solids using plasmonic nanoparticle arrays. *Sens. Actuators, B* **2010**, *150*, 667–672.

(12) Morris, T.; Kloepper, K.; Wilson, S.; Szulczewski, G. A spectroscopic study of mercury vapor adsorption on gold nanoparticle films. *J. Colloid Interface Sci.* **2002**, *254*, 49–55.

(13) James, J. Z. *Mercury sensing with optically responsive gold nanoparticles*. Ph.D. Dissertation, UC Berkeley, Berkeley, CA, 2012.

(14) Braman, R. S.; Johnson, D. L. Selective absorption tubes and emission technique for determination of ambient forms of mercury in air. *Environ. Sci. Technol.* **1974**, *8*, 996–1003.

(15) Levlín, M.; Ikävalko, E.; Laitinen, T. Adsorption of mercury on gold and silver surfaces. *Fresenius' Journal of Analytical Chemistry* **1999**, *365*, 577–586.

(16) Grzelczak, M.; Perez-Juste, J.; Mulvaney, P.; Liz-Marzan, L. M. Shape control in gold nanoparticle synthesis. *Chem. Soc. Rev.* **2008**, *37*, 1783–1791.

(17) Link, S.; Wang, Z. L.; El-Sayed, M. A. Alloy formation of gold–silver nanoparticles and the dependence of the plasmon absorption on their composition. *J. Phys. Chem. B* **1999**, *103*, 3529–3533.

(18) Tao, A. R.; Huang, J.; Yang, P. Langmuir–Blodgett of nanocrystals and nanowires. *Acc. Chem. Res.* **2008**, *41*, 1662–1673.

(19) Jain, P. K.; Huang, W.; El-Sayed, M. A. On the universal scaling behavior of the distance decay of plasmon coupling in metal nanoparticle pairs: A plasmon ruler equation. *Nano Lett.* **2007**, *7*, 2080–2088.

(20) Sendroiu, I. E.; Mertens, S. F. L.; Schiffrin, D. J. Plasmon interactions between gold nanoparticles in aqueous solution with controlled spatial separation. *Phys. Chem. Chem. Phys.* **2006**, *8*, 1430–1436.

(21) Tao, A.; Sinsermsuksakul, P.; Yang, P. Tunable plasmonic lattices of silver nanocrystals. *Nat Nano* **2007**, *2*, 435–440.

(22) Buffat, P.; Borel, J.-P. Size effect on the melting temperature of gold particles. *Phys. Rev. A* **1976**, *13*, 2287–2298.

(23) Slemr, F.; Brunke, E.-G.; Ebinghaus, R.; Kuss, J. Worldwide trend of atmospheric mercury since 1995. *Atmos. Chem. Phys.* **2011**, *11*, 4779–4787.

(24) Mirsky, V. M.; Vasjari, M.; Novotny, I.; Rehacek, V.; Tvarozek, V.; Wolfbeis, O. S. Self-assembled monolayers as selective filters for chemical sensors. *Nanotechnology* **2002**, *13*, 175.